Capture barrier distributions: Some insights and details

N. Rowley, N. Grar, M. Trotta

Capture barrier distributions: some insights and details

N. Rowley

Institut Pluridisciplinaire Hubert Curien (UMR 7178: CNRS/ULP),
23 rue du Loess, F-67037 Strasbourg Cedex 2, France

N. Grar

Department of Physics, University of Sétif, Algeria

M. Trotta

INFN, Sezione di Napoli, I-80126, Italy
(Dated: September 28, 2007)

The 'experimental barrier distribution' provides a parameter-free representation of experimental heavy-ion capture cross sections that highlights the effects of entrance-channel couplings. Its relation to the s-wave transmission is discussed, and in particular it is shown how the full capture cross section can be generated from an $l = 0$ coupled-channels calculation. Furthermore, it is shown how this transmission can be simply exploited in calculations of quasi-fission and evaporation-residue cross sections. The system ^{48}Ca + ^{154}Sm is studied in detail. A calculation of the compound-nucleus spin distribution shows up a possible energy dependence of barrier weights due to polarization arising from target and projectile quadrupole phonon states; an effect which also gives rise to an entrance-channel 'extra-push'.

I. INTRODUCTION

The complexity of heavy-ion reactions depends to a large extent on the charge product $Z_1 Z_2$ of the colliding nuclei. However, for all but the very highest-$Z_1 Z_2$ reactions, the first stage in the creation of a composite system is determined by the crossing of an external Coulomb barrier, or in the case of strong entrance-channel couplings, a "distribution of barriers". This stage of the reaction is referred to as "capture" or sometimes "barrier-crossing". For very heavy systems such as Pb + Pb, this will clearly not be true, since there will be a significant overlap of the nuclear densities before the Coulomb barrier is reached. This will lead to strong dissipative effects and an important flow of nucleons between the colliding nuclei. However, recent experiments have shown [1, 2] that even for systems of the type leading to superheavy-element creation by cold fusion, the concept of a distribution of external Coulomb barriers is still valid. The results of this paper should apply to any collision where this is the case.

For light and intermediate-mass reactions, the composite system will evolve to form an equilibrated, compact compound nucleus (CN). This we refer to as "fusion". The CN will then cool by the emission of light particles (neutrons, protons and α-particles) to create long-lived evaporation residues (ER). For heavier, composite systems an increasing fraction of the capture cross section $\sigma_{\rm cap}$ will undergo quasi-fission (QF) before CN formation. Furthermore the CN itself may fission (fusion-fission; FF). Thus the experimental difficulties in measuring $\sigma_{\rm cap}$ increase with $Z_1 Z_2$; for this reason, the experiments [1, 2] mentioned above determined the capture barrier distribution from the large-angle quasi-elastic scattering [3]. In the present paper, we wish to discuss the properties of the capture cross section and the extent to which it can be represented as a distribution of barriers. The consequences of this on other cross sections will also be explored.

The "experimental barrier distribution" was introduced in Ref. [4] as

$$D(E) \equiv \frac{1}{\pi R^2} \frac{d^2(E\,\sigma_{\rm cap})}{dE^2}, \qquad (1)$$

where E is the center-of-mass energy and R is some average barrier radius chosen simply to normalize the area of $D(E)$ to unity. (Note that this was referred to as the "fusion" barrier distribution, since fusion and capture were identical in the systems originally discussed. Here we shall refer to it as the "capture" barrier distribution, or simply the barrier distribution.) For the classical capture cross section from a single barrier, Eq. (1) gives [4, 5]

$$D_{\rm class}(E) = \delta(E - B), \qquad (2)$$

where B is the barrier height. In the single-barrier quantum mechanical problem [5], D is more generally a function having unit area strongly peaked at $E = B$.

The quantity $D(E)$ frequently possesses detailed structures [5] that reflect the presence of different barriers generated by coupling to the collective excitations of the target and projectile in the entrance channel. Transfer channels may also play an important role [6]. It can also be shown [7, 8] that the first derivate of $E\,\sigma_{\rm cap}$ has a physical interpretation in terms of the total s-wave transmission in the entrance channel

$$T_0^{\rm tot} \approx \frac{1}{\pi R^2} \frac{d(E\,\sigma_{\rm cap})}{dE}. \qquad (3)$$

(We shall use the symbol T_0 for a single, uncoupled barrier.)

It is important to note here that Eq. (1) is simply a definition. That is, it defines a function of the experimental data in which the dynamics is accentuated and as such it is very useful for comparisons with theory. However, it contains no more information than the primary data themselves, though its name implies that one can approximately write

$$\sigma_{\text{cap}} \approx \sum_\alpha w_\alpha \, \sigma_{\text{cap}}(E, B_\alpha), \qquad (4)$$

where w_α and B_α are the weights (probabilities) and heights of the barriers contained in the distribution. Indeed this relation can be proved analytically but only under certain restrictive conditions. These are essentially [5]: the isocentrifugal approximation for the centrifugal potential; zero excitation energies for the coupled collective states (sudden approximation, where the intrinsic nuclear states may be considered as 'frozen' during the collision); and the same form factor for all the couplings. Despite the fact that these conditions are not always well fulfilled (in particular for phonon excitations, the sudden approximation is far from valid) the experimental data still generally present well defined structures which can often be fitted by appropriate coupled-channels calculations. Therefore, one aim of the present paper is to study the extent to which the above expression (4) is more generally true and how it might be further exploited.

We shall also examine in detail the relationships between σ_{cap}, T_0^{tot} and $D(E)$ and show that there are various useful consequences of these. In particular we shall show that we can obtain an excellent approximation to the full capture cross section from a coupled-channels calculation for just $l = 0$. Under certain assumptions we shall also show how this may be extended to approximate calculations for the quasi-fission and evaporation-residue cross sections. However, an attempt to simplify the calculation of CN spin distributions reveals that it may sometimes be necessary to account explicitly for the energy dependence of the barrier weights w_α.

II.   CAPTURE DYNAMICS AND T_0^{tot}

The interpretation of $D(E)$ in terms of a set of Coulomb barriers is clear. However, the quantity T_0^{tot} also has some very useful properties. This is demonstrated in Fig. 1 for data on the ^{100}Mo + ^{100}Mo taken by Quint et al. [9]. (Parts (a) and (b) are the same but shown on logarithmic and linear scales.) It is important to note that in this, and in many similar experiments, only the total evaporation-residue cross sections σ_{ER} were measured. The data points for the s-wave transmission were calculated for the gaussian barrier distribution required to fit the ER cross section in a HIVAP calculation [10]. Thus it is not parameter-free as it would
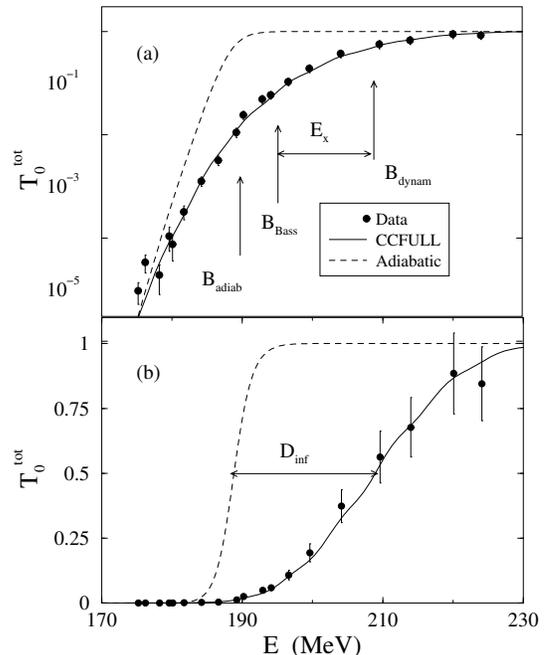

FIG. 1: The experimental T_0^{tot} of Quint et al. [9] for ^{100}Mo + ^{100}Mo demonstrates the concepts of the dynamical and adiabatic barriers, and of D_{inf} and the extra-push energy E_{x}. The solid curve shows the fit of Ref. [12] to these data, and the dashed curve shows a single barrier cross section which fits the lowest-energy points. Parts (a) and (b) show the same curves on logarithmic and linear scales respectively.

be if taken from a derivative of the capture cross section directly (not known in this case). It is, nonetheless a useful way of displaying experimental results.

One can immediately read off the energy of the average, or "dynamical" barrier B_{dynam}, at which $T_0^{\text{tot}} = 0.5$, and the energy of the "adiabatic" barrier B_{adiab} for which a single-barrier cross section reproduces the data at the lowest energies. The difference between the dynamical barrier and some expected, nominal barrier (for example the Bass barrier B_{Bass} [11]) shows that there is an 'extra-push' energy $E_{\text{x}} = B_{\text{dynam}} - B_{\text{Bass}}$ in this and similar systems. On the other hand, the quantity $D_{\text{inf}} = B_{\text{dynam}} - B_{\text{adiab}}$ provides a useful measure of the width of the barrier distribution.

The data shown in Fig. 1 have recently been re-analyzed in terms of the multi-phonon couplings in the entrance channel for this and other symmetric, or almost symmetric, systems [12]. The overall shape of T_0^{tot}, thus D_{inf} can be fitted with such calculations and the couplings also account for most of the extra-push energy (see Sect. VI) without invoking extra internal barriers [13]. The calculations are difficult, since for high $Z_1 Z_2$ and many channels, they become numerically unstable at low E. The situation is helped by the fact that the data had been represented simply as T_0^{tot}, since this allows one to solve the coupled-channels equations for a single partial wave. We wish to show how the full capture cross section

can be rather well obtained from such a calculation.

III. RELATING T_0^{tot}, σ AND D

A. Single barrier

Henceforth we shall simply use the symbol σ for the capture cross section. The symbol σ_l will refer to the partial capture cross section for a given l value (particularly σ_0 for the s-wave). Other physical cross sections will take an appropriate suffix.

For a single barrier we may write the s-wave transmission coefficient very generally as

$$T_0 \equiv T_0(E - B). \tag{5}$$

For a system of reduced mass m, the partial cross section for $l = 0$ is related to T_0 by

$$E\,\sigma_0 = \left(\frac{\pi\,\hbar^2}{2m}\right) T_0(E - B) \tag{6}$$

and the total cross section given by

$$E\,\sigma = \left(\frac{\pi\,\hbar^2}{2m}\right) \sum_{l=0}^{\infty} (2l + 1)\, T_l(E - B). \tag{7}$$

We may now follow the steps of Wong [14], used to derive the total cross section from the transmission through a parabolic barrier. Note, however, that we make no assumption concerning the particular form of the transmission function T which will depend on the shape of the potential.

First we replace T_l by $T_0(E' - B)$, with

$$E' = E - \frac{l(l + 1)\,\hbar^2}{2mR^2}. \tag{8}$$

That is, we approximate the centrifugal potential by its value at the barrier radius R. Thus

$$E\,\sigma \approx \left(\frac{\pi\,\hbar^2}{2m}\right) \sum_{l=0}^{\infty} (2l + 1)\, T_0(E' - B). \tag{9}$$

Replacing the sum by an integral we have

$$E\,\sigma \approx \left(\frac{\pi\,\hbar^2}{2m}\right) \int_0^{\infty} (2l + 1)\, T_0(E' - B)\, dl \tag{10}$$

and using the expression (8) for E' we may write the rather general relation between the s-wave transmission and the total cross section σ

$$E\,\sigma \approx \pi R^2 \int_0^{E} T_0(E' - B)\, dE', \tag{11}$$

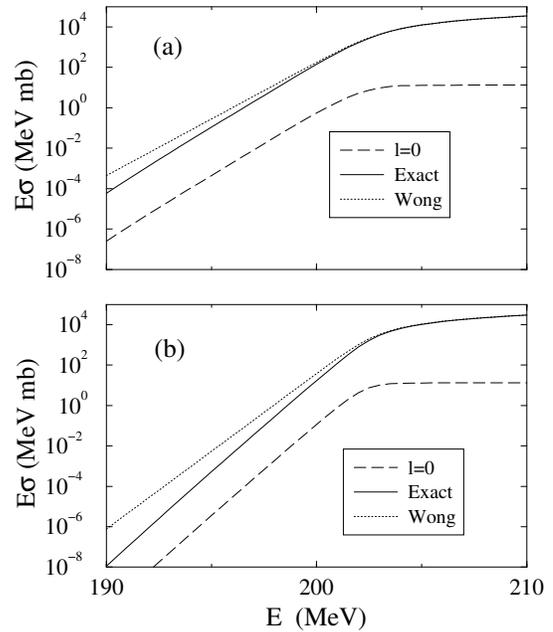where the radius R is taken to have its s-wave value but no reference has been made to the particular shape of the

FIG. 2: For ^{100}Mo $+$ ^{100}Mo and a single barrier with $B = 202.4$ MeV, we show $E\sigma_0$ and $E\sigma$, where σ_0 and σ are the exact optical-model s-wave partial cross section (dashed curve) and total capture cross section (solid curve) respectively. The results of Eq. (11) are practically indistinguishable from the exact results on this scale: (a) corresponds to a surface diffuseness $a = 0.6$ fm and (b) to $a = 1.2$ fm. Note the significant deviations in the Wong cross sections below the barrier (dotted curves) using a curvature calculated at the barrier top.

barrier. In particular, the barrier "curvature" $\hbar\omega$ does not occur explicitly in this equation.

If, however, we use the Hill-Wheeler approximation for a parabolic barrier with this curvature,

$$T_0 = \frac{1}{1 + \exp(2\,\pi[B - E]/\hbar\omega)}, \tag{12}$$

then Eq. (11) yields the well known Wong cross section [14]

$$E\,\sigma = \frac{1}{2}\hbar\,\omega\,R^2 \ln(1 + \exp(2\,\pi[E - B]/\hbar\omega)). \tag{13}$$

Eq. (11) should, however, be more generally applicable and we shall first test it with an optical-model calculation.

Fig. 2 shows the results of (uncoupled) optical-model calculations with a real potential which is essentially exponential in the tail and having a diffuseness of (a) $a = 0.6$ fm and (b) $a = 1.2$ fm. In both cases the barrier height is $B = 202.4$ MeV and the Coulomb potential corresponds to ^{100}Mo $+$ ^{100}Mo. The imaginary potential is confined to the nuclear interior to simulate a pure ingoing-wave boundary condition. The dashed curves show the $E\sigma_0$ obtained by a solution of the Schroedinger equation. The solid curve shows the corresponding $E\sigma$.
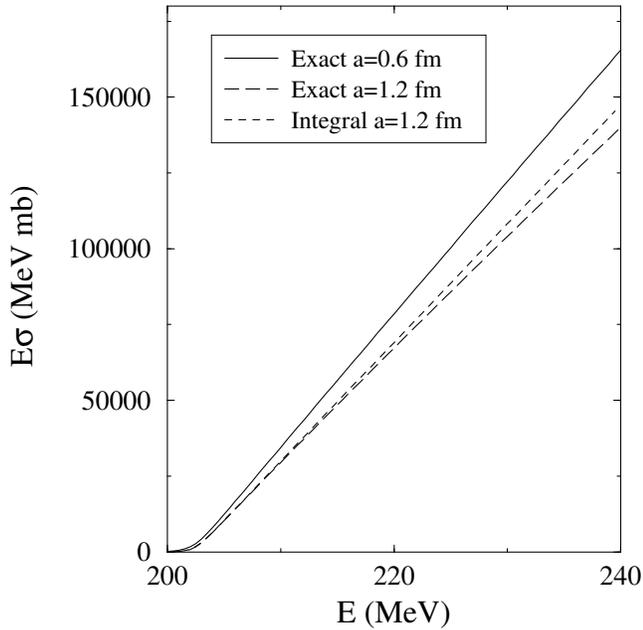
FIG. 3: The same quantities as in Fig. 2 on a linear scale and at higher E. For $a = 0.6$ fm the integral (11) is almost indistinguishable from the exact results and is not shown. For $a = 1.2$ fm there are small differences due to the fact that the barrier for high l values shifts to smaller radii. In this respect, the Wong cross section gives a very similar result to the integral.

(Throughout this paper, cross sections will be represented as $E\sigma$ in units of MeV mb.) The cross section derived from Eq. (11) is indistinguishable from the exact result on this scale. The dotted curves show the Wong cross section (13). One can see that the cross section falls more rapidly for the larger diffuseness and that the discrepancies between Wong and the exact calculation become very large at deep sub-barrier energies [15]. This discrepancy is probably best quantified by the logarithmic derivative of the low-E cross section (see Sect. III D). In both cases, however, the relation (11) gives excellent results. The integration in that equation was performed using Simpson's rule. We use an integration step of 0.2 MeV throughout the paper.

Thus we have reduced the calculation of a full capture cross section to solving the Schroedinger equation for a single l value. This is not a particularly important achievement for a simple optical-model calculation but it could be of enormous benefit if it can be extended to coupled-channels calculations, where the time taken for each l value may be relatively long, and the calculation may become numerically unstable for large angular momentum values.

Fig. 3 shows $E\sigma$ for the two values of diffuseness on a linear scale at energies well above the barrier. For $a = 0.6$ fm the integral is still almost indistinguishable on this scale from the exact results. For the larger diffuseness, the curve has a smaller slope since the bar-

rier radius must be smaller if we are to maintain the same barrier height of 202.4 MeV ($R_{0.6} = 11.91$ fm and $R_{1.2} = 10.72$ fm; see Eq. (22)). Now a small discrepancy shows up between the integral and the exact results since the barrier position is l-dependent and this dependence increases with increasing diffuseness [16]. We note that the s-wave barrier is a-dependent and that this essentially gives a first-order correction to the cross section. This is correctly accounted for by the above formalism. In addition, however, there is a second-order effect which depends on l as well as the diffuseness. This is not accounted for, and we shall not pursue this further in the present paper.

B. Several barriers: variation of the barrier radius

Eq. (4) implies that we can write a similar weighted sum for the total s-wave transmission T_0^{tot}

$$T_0^{\text{tot}}(E) = \sum_\alpha w_\alpha \, T_0(E - B_\alpha). \qquad (14)$$

Following the above derivation of Eq. (11), we now find

$$E\,\sigma \approx \pi \sum_\alpha \int_0^E R_\alpha^2 w_\alpha \, T_0(E' - B_\alpha) \, dE' \qquad (15)$$

and if one sets all the R_α equal to a common value R, one recovers Eq. (11), which now relates the total capture cross section (summed over all l) to the total s-wave transmission (summed over all barriers):

$$E\,\sigma \approx \pi R^2 \int_0^E T_0^{\text{tot}}(E') \, dE'. \qquad (16)$$

For small deformations of target and projectile, the above approximation of a fixed R is reasonable. However, for large deformations, there may be relatively large differences in the positions of the different Coulomb barriers and this may lead to some errors in extracting the total cross section from a calculation with $l = 0$. We can, however, circumvent this problem by noting that the derivative of the s-wave transmission coefficient is strongly peaked at $E = B$ for each barrier. Thus if we have an analytic expression for $R_\alpha \equiv R(B_\alpha)$ we may write

$$\frac{d}{dE'} \sum_\alpha w_\alpha R_\alpha^2 \, T_0^\alpha(E') \approx R^2(E') \frac{dT_0^{\text{tot}}(E')}{dE'} \qquad (17)$$

with $T_0^\alpha(E') \equiv T_0(E' - B_\alpha)$. Thus the integrand of Eq. (15) may be written

$$\sum_\alpha w_\alpha R_\alpha^2 \, T_0^\alpha(E') \approx \int_0^{E'} R^2(B) \frac{dT_0^{\text{tot}}(B)}{dB} \, dB, \qquad (18)$$

where we use the integration variable B to emphasize the fact that this integral is equivalent to the sum over the

barriers α. Finally this gives

$$E\,\sigma \approx \pi \int_0^E \int_0^{E'} R^2(B) \frac{dT_0^{\text{tot}}(B)}{dB}\, dB\, dE' \qquad (19)$$

and we have again achieved our aim of expressing the total capture cross section for all l in terms of that simply for $l = 0$. The integral over E' is equivalent to the sum over l as in Eq. (11).

In both expressions (16) and (19), all of the information on the channel couplings (that is, on the barrier distribution (w_α, B_α)) is contained in the single function T_0^{tot}, which can be obtained from a single calculation with $l = 0$. We have passed from the single integral of Eq. (16) to the double integral (19) in order account for the variation of R_α for the different barriers, since dT_0/dE is peaked for each barrier. However, more importantly, this will also allow us to introduce into the integrand of Eq. (19) *any other function* of the barrier position B. In particular we shall later introduce the possibility of a quasi-fission component of the reaction which is barrier dependent due to the "compactness" [17] of the configuration at the barrier.

Since the Coulomb barrier will almost always occur in the region where the nuclear potential is approximately exponential, it is relatively easy to obtain an expression for $R(B)$. At the barrier $V_C' + V_N' = 0$, and since V_N is exponential,

$$V_N(R) = -a \frac{Z_1 Z_2\, e^2}{4\pi\varepsilon_0\, R^2} \equiv -a \frac{Z}{R^2} \qquad (20)$$

and thus $V_C' + V_N' = 0$ yields

$$B = \frac{Z}{R}\left(1 - \frac{a}{R}\right). \qquad (21)$$

Solving this quadratic equation for R we obtain

$$R(B) = \frac{Z}{2B}\left(1 + \left[1 - \frac{4aB}{Z}\right]^{1/2}\right). \qquad (22)$$

For small a, the approximation $R(B) = Z/B - a$ may be adequate, but in mapping from an $l = 0$ calculation to the full cross section, we shall use the more exact relation (22) in the double integral of Eq. (19).

Of course we have again achieved little in the case where we have an expression in the form of Eq. (14) and know the values the the barrier heights B_α and their weights w_α. However, Eq. (19) contains no reference to these, which are in any case not a natural output of a coupled-channels calculation. Indeed the very existence of eigenchannels assumed in Eqs. (4,14) can be proved only under the very restricted conditions mentioned in the introduction. However, we note that in Eq. (19) there is no reference to eigenchannels, or weights, or barrier heights, and we may hope that it will, therefore, apply more generally to results from coupled-channels calculations.
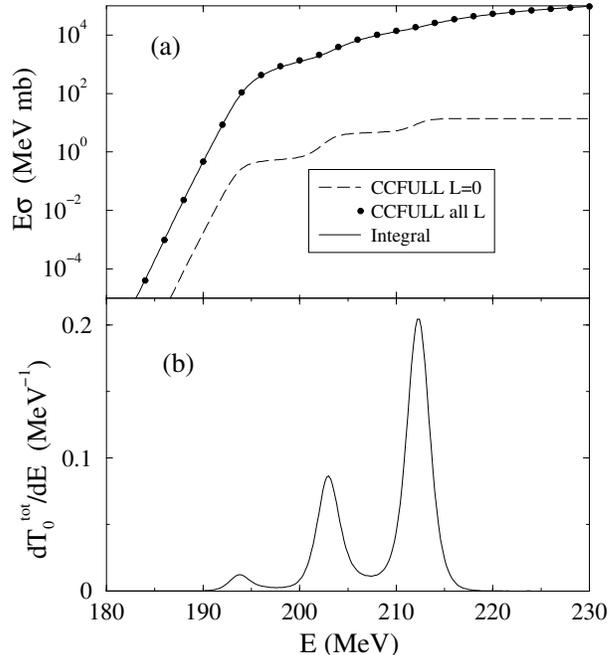

FIG. 4: (a) For ^{100}Mo + ^{100}Mo with coupling to the first quadrupole-phonon state in each nucleus [1,1], we show $E\sigma_0$ (dashed curve) and $E\sigma$ (circles) both calculated with CC-FULL. The results of Eq. (19) are shown by the solid line. (b) Shows the corresponding 'barrier distribution' dT_0^{tot}/dE.
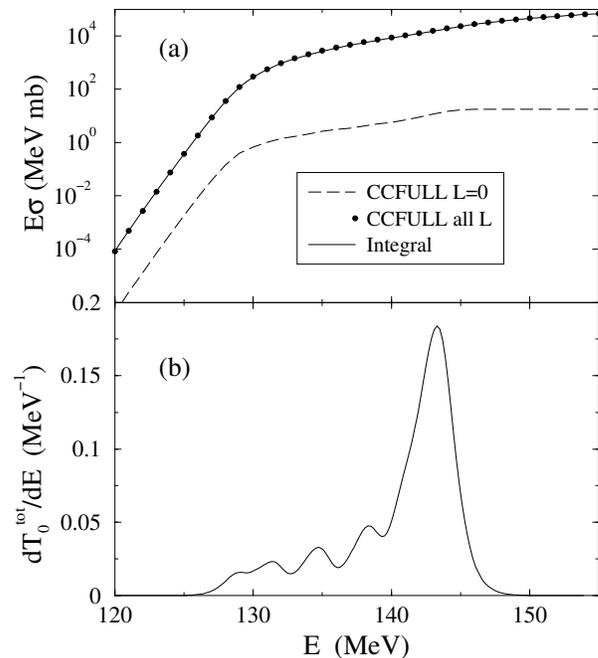

FIG. 5: Same quantities as in Fig. 4 but for the system ^{48}Ca + ^{154}Sm with quadrupole couplings to the first six excited states [0,6] of the ^{154}Sm ground-state rotational band (0^+ to 12^+).

Throughout the rest of this paper we shall present a

number of coupled-channels calculations to demonstrate our results. These will all use a nuclear potential which is essentially exponential in the barrier region with a surface diffuseness $a = 0.6$ fm. The potential is, therefore, uniquely specified by quoting the barrier height B_{nc} with no coupling. For the channel couplings, we shall take throughout a coupling radius $r_0 = 1.20$ fm. Couplings are, therefore, completely specified by the excitation energies $E_{I\pi}$ of the states concerned (spin I and parity π), the corresponding deformation parameters of the states β_L, and by the number of excited states (rotational or vibrational) included in the calculations. These are denoted $[N_{\text{projectile}}, N_{\text{target}}]$. Thus an uncoupled calculation would be denoted $[0,0]$.

It can be seen in Figs. 4, 5 that the expression (19) works extremely well. Fig. 4 shows results for the vibrational system ^{100}Mo + ^{100}Mo with coupling to the first quadrupole-phonon state ($E_{2^+} = 0.53$ MeV; $\beta_2 = 0.23$) in each nucleus and $B_{nc} = 202.4$ MeV. (This $[1,1]$ coupling scheme is a truncation of the more physical couplings used in Ref. [12], and whose results are shown in Fig. 1. This clearly will not fit the experimental data but the fact that it gives rise to discrete barriers will facilitate some of our later discussions.) The dashed curve in part (a) of the figure shows $E\sigma_0$ calculated using the program CC-FULL [18]. The open circles show the full $E\sigma$ calculated using the same program but including up to $l = 100$. The solid curve shows the $E\sigma$ generated from the s-wave calculation using Eq.(19), and can be seen to give excellent results. Part (b) of the figure shows the 'barrier distribution' defined as dT_0^{tot}/dE (see next subsection III C).

Fig. 5 shows all the same quantities as Fig. 4 but now for the system ^{48}Ca + ^{154}Sm with quadrupole coupling ($\beta_2 = 0.30$, $\beta_4 = 0.05$) to the first six excited rotational states of the ^{154}Sm ground-state rotational band (that is up to the 12^+ state) and an inert ^{48}Ca (coupling $[0,6]$). The 2^+ state has energy 82 keV and the other energies were taken to follow an $I(I + 1)$ law. Eq. (19) is again seen to give excellent results. This system is discussed in more detail in Sect. IV.

For very heavy ions, one may have to consider hundreds of partial waves to obtain convergence of the capture cross section and some problems of stability of the CC calculations may arise, since for the higher partial waves the energy in question may be very far below the total potential barrier. Furthermore, the performance of coupled-channels calculations becomes time consuming for many channels and reducing this to a single calculation for $l = 0$ has very obvious benefits. The calculation of the double integral in Eq. (19) is very rapid, even compared with solving the coupled equations for just a single l. This is especially important when trying to optimize parameters to fit experimental data. Note also that we need to calculate only up to energies where dT_0^{tot}/dE becomes 0, even if we require cross sections above this energy.

C. Defining the barrier distribution

The most natural mathematical definition of the barrier distribution is dT_0^{tot}/dE since for a single barrier it gives a function normalized to 1 and peaked at $E = B$. Thus for many barriers we obtain a sum of functions each having a weight w_α and peaked at B_α. From Eq. (19) we see that this is equal to

$$D(E) = \frac{d}{dE}T_0^{\text{tot}}(E) = \frac{1}{\pi R^2(E)}\frac{d^2(E\sigma)}{dE^2}. \qquad (23)$$

Apart from the E-dependence of R (actually a B-dependence), this is of course the usual definition [4] of the 'experimental barrier distribution' (1).
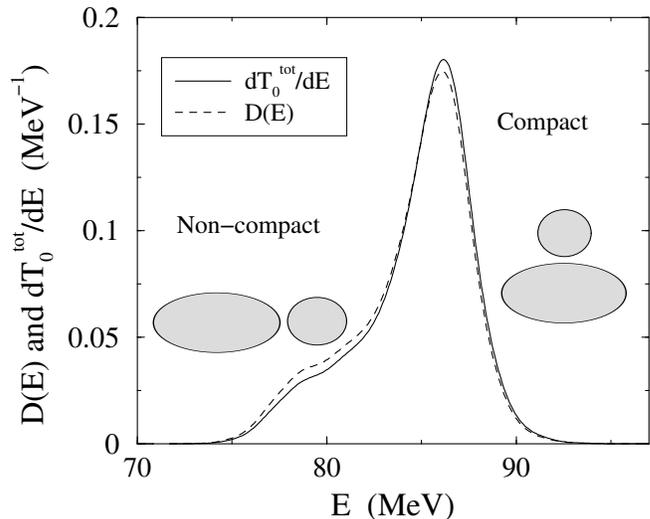
FIG. 6: For the system ^{16}O + ^{238}U we show the difference between including the barrier-dependence of the radius and ignoring it (see Eq. (24)). Both curves are normalized to unity. The insets show schematically how the high barriers correspond to a more 'compact' configuration than the low ones (see Sect. IV B).

We do not, however, suggest the inclusion of such an energy dependence in the experimental results, since this involves introducing an unknown theoretical parameter a. Dividing the second derivative by a fixed πR^2 merely introduces a harmless overall normalization.

Of course whatever one does to the data should also been done to a calculation before a comparison is made. So the second derivative of the theoretical $E\sigma$ of Eq. (19) should be treated in the same way as its experimental equivalent. However, in this paper we wish to advocate simplified CC calculations using only $l = 0$. In that case we simply note that

$$\frac{d^2(E\sigma)}{dE^2} = \pi R^2(E)\frac{dT_0^{\text{tot}}(E)}{dE}. \qquad (24)$$

Now the barrier-dependence of R can be simply included since the value of the diffuseness used in the calculations is known.

Fig. 6 shows the difference between dT_0^{tot}/dE and the usual 'experimental barrier distribution' of Eq. (1), with R chosen so that $D(E)$ is also normalized to unity for the system ^{16}O + ^{238}U (calculated with $E_{2+} = 45$ keV, β_2=0.275, β_4=0.05). The differences are seen to be relatively small, which means that for most purposes, the single integral of Eq. (16) will give good results. However, a major advantage of the double integral of Eq. (19) is that we can also introduce into it other functions of B. We shall demonstrate this in Sect. IV where we shall introduce quasi-fission through the notion of 'compactness' [17].

D. Logarithmic derivative

It has been noted recently that at deep sub-barrier energies, many heavy-ion fusion cross sections fall off anomalously rapidly (see for example, Refs. [19–21]). This phenomenon is perhaps best displayed through the logarithmic derivative of the cross section which becomes slowly varying at these energies, at values consistent with a greater surface diffuseness than considered normal. For example, Dasgupta [21] shows that in the system ^{16}O + ^{208}Pb, the experimental $d\ln(E\sigma)/dE$ is consistent with a value of a=1.65 fm. However, the behavior of the cross section at high energies appears to require a different value of a (c.f. Fig. 3).
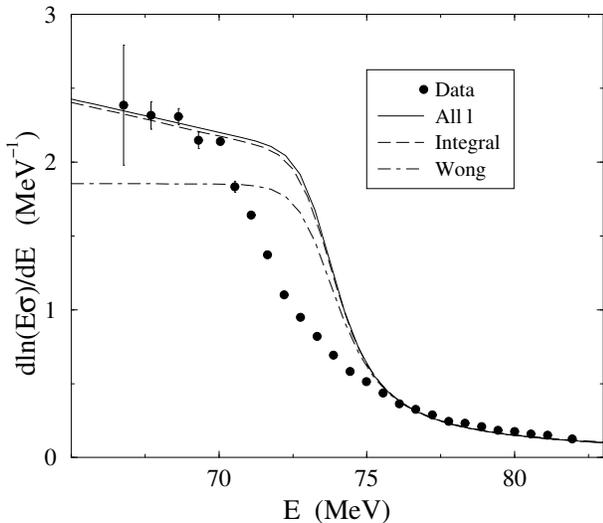

FIG. 7: The expression (11) reproduces very well the logarithmic derivative far below the Coulomb barrier. This is an uncoupled calculation for ^{16}O + ^{208}Pb with a =1.65 fm. The Wong approximation does not reproduce the correct behavior in this energy region.

We do not attempt to provide an explanation of this phenomenon but merely wish to show here that an integral expression is capable of reproducing the cross section sufficiently well at these low energies if one wishes to study this property. Using Eq. (11), we may write for a single barrier

$$\frac{d\ln(E\,\sigma)}{dE} = \frac{d}{dE}\ln \int_0^E T_0(E')dE' \equiv \frac{T_0(E)}{\int_0^E T_0(E')dE'}. \quad (25)$$

Fig. 7 reproduces the Fig. 7 of Dasgupta from Ref. [21] for a single uncoupled barrier in ^{16}O + ^{208}Pb. There is no attempt here to fit the data except the logarithmic derivative at the lowest energies. We see that the results from the integral formalism again agree extremely well with a calculation including all l values. The Wong approximation, however, fails in this region. One may easily show from Eq. (13) that the Wong value saturates at $2\,\pi/\hbar\omega$, which is 1.85 MeV^{-1} in this case.

For a single potential barrier, certain analytic expressions exist within the WKB approximation which allow the inversion of the barrier penetration to yield the barrier thickness, and thus the form of the potential itself [22]. Early applications [23] of this technique to heavy-ion fusion cross sections yielded rather unphysical, often multi-valued potentials, since the cross section actually comes from a distribution of barriers. It has very recently [24] been shown, however, that in certain circumstances (essentially where the lowest barrier is dominant), one may take account of this fact and perform the inversion more correctly. In particular the above case of ^{16}O + ^{208}Pb is susceptible to such a treatment. The potential thus obtained is well behaved but rather different from most 'standard' heavy-ion potentials. It remains to be seen if a theoretical justification for the new shape can be found, or whether the potential (albeit well behaved) still mocks up some other, missing, physical effect.

IV. OTHER PHYSICAL PROPERTIES

A. General comments

We have seen how the total capture cross section

$$\sigma = \frac{\pi}{k^2} \sum_{l=0}^{\infty} (2l + 1)\, T_l \quad (26)$$

can be approximately represented in terms of an integral containing simply the transmission coefficient T_0^{tot} for the s-wave. Eq. (16) contains a single integral over E' which replaces the above sum over the partial waves. Eq. (19), however, contains a second integral over B which formally represents a sum over different Coulomb barriers.

These results can be simply extended to other physical quantities such as the fusion-fission cross section, the quasi-fission cross section and the fusion-evaporation cross section. For example the quasi-fission cross section may be written

$$\sigma_{\text{QF}} = \frac{\pi}{k^2} \sum_{l,\alpha} (2l+1)w_\alpha\, T_l(E, B_\alpha)\, P_{\text{QF}}(l, E, \alpha), \quad (27)$$

where $P_{QF}(l, E, \alpha)$ is the probability of quasi-fission, and we have expressed this cross section as a sum over barriers since, as pointed out by Hinde et al. [17], P_{QF} may depend on the 'compactness' of the composite system which in turn depends on the barrier configuration. This is schematically shown by the shaded inserts in Fig. 6, where we see that for a spherical projectile on a deformed target, the low-energy barriers correspond to a 'non-compact' collision with the tip of the target, whereas the high-E barriers correspond to a more compact collision with the equator.

Since quasi-fission reduces the compound nucleus cross section, the total evaporation-residue cross section may be written:

$$\sigma_{ER} = \frac{\pi}{k^2} \sum_{l,\alpha} (2l+1) w_\alpha \, T_l(E, B_\alpha) \qquad (28)$$
$$\times (1 - P_{QF}(l, E, \alpha)) P_{sur}(l, E^*),$$

where the survival probability is related to the fusion-fission probability by $P_{sur}(l, E^*) = (1 - P_{fiss}(l, E^*))$, and depends on the excitation energy E^* of the compound nucleus, which is of course just given by $E^* = E + Q$, with Q the reaction Q-value. In both of the above cases, the probability functions can easily be incorporated into the integral formalism (19) so that again the entrance-channel dependence is given by the single function T_0^{tot}.

Since the purpose of the present article is essentially to demonstrate the principles involved in this concept, we shall limit ourselves to the two simple examples given below, both for the system ^{48}Ca + ^{154}Sm, where all three cross sections σ_{cap}, σ_{ER} and σ_{QF} have been measured independently [25, 26].

B. Compactness: cross section for quasi-fission

Different mechanisms have been proposed for the possible failure to form a compound nucleus following the crossing of the potential barrier (see, for example, Refs. [13, 27]). However, to demonstrate the usefulness of the expression (19) we shall discuss here only the compactness notion of Hinde et al. [17]. In its simplest prescription, the composite system is assumed to fuse if the angle between the separation vector and the symmetry axis of the deformed nucleus exceeds a certain value. This of course means if the barrier height B exceeds a certain value. This is, however, somewhat extreme. In the case of the above system ^{48}Ca + ^{154}Sm, it was noted that at low energies σ_{QF} is around 20% of σ_{cap}. However, at higher energies it becomes a smaller fraction of this. Thus we may retain the spirit of the compactness concept with a more general parametrization of $P_{QF}(\alpha)$ with the Fermi-function form:

$$P_{QF}(\alpha) \equiv P_{QF}(B) = \gamma_{QF} \frac{1}{1 + \exp(\frac{B - B_{QF}}{\Delta_{QF}})}. \qquad (29)$$

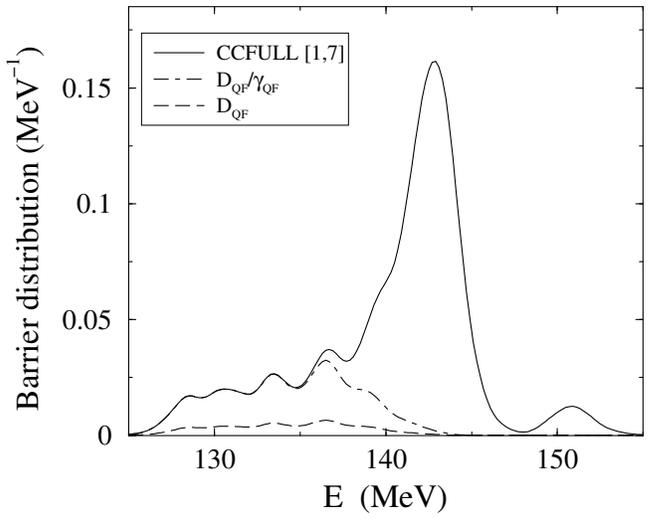That is, there is a fraction γ_{QF} of QF for the non-compact barriers, reducing to zero for the more compact ones.

FIG. 8: The calculated capture barrier distribution is shown for the [1,7] ^{48}Ca + ^{154}Sm calculation described in the text. The dot-dashed line shows the part of this distribution which contributes to quasi-fission, and the dashed curve is the QF barrier distribution used, including the factor $\gamma_{QF} = 0.2$ (see text and Fig. 9)
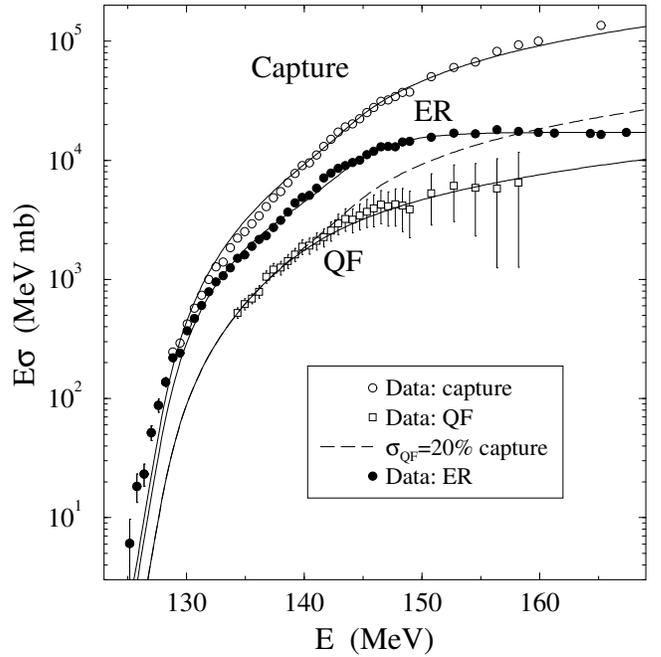

FIG. 9: The measured and calculated capture, quasi-fission and evaporation-residue cross sections for ^{48}Ca + ^{154}Sm (see text and Figs 8, 10 for more details).

The solid line in Fig. 8 shows our calculated capture barrier distribution, and in Fig. 9, we compare the corresponding capture cross section with the experimental data. The fit uses the same parameters as in Fig. 5 but a slightly better fit at the lowest energies is obtained by taking up to 7 excited states of the ^{154}Sm rotational band

(that is, up to the 14^+ state). Furthermore, there is a relatively important effect of the inclusion of the 3^- octupole phonon state in the ^{48}Ca, which introduces an additional barrier at around 151 MeV (c.f. Fig. 5) and pushes the previous barriers down slightly in energy (c.f. Fig. 5). With this latter state included, we require an uncoupled barrier $B_{\rm nc}=140.9$ MeV, just 1.8 MeV higher than $B_{\rm Bass} = 139.1$ MeV, in order to obtain a reasonable fit to the data.

The dashed line in Fig. 8 shows the part of the distribution corresponding to quasi-fission with $\gamma_{\rm QF}=0.2$, $B_{\rm QF}=138.5$ MeV and $\Delta_{\rm QF} =1.0$ MeV. The corresponding cross section is shown in Fig. 9, and is simply obtained by inserting the above expression (29) into Eq. (19). (Eq. (11) is of no use here since we must integrate over all barriers.) The procedure is seen to give a good fit to the experimental data, whereas a constant fraction of 20% QF (dashed curve in Fig.9) greatly over-predicts the cross section at higher energies. The parameters $B_{\rm QF}$ and $\Delta_{\rm QF}$ describe the way that the QF is cut off for the compact barriers (dot-dash curve in Fig.8) which proceed essentially to CN creation. While the values of these parameters are not precisely determined by the experiment, the data may certainly be said to require around 20% QF for the low barriers and very little from the highest ones, confirming the compactness notion in this system.

High above a particular barrier we may write $E\sigma \approx \pi R^2 (E - B)$, so that at energies above all the barriers, this model gives a constant ratio of the QF and capture cross sections: $\sigma_{\rm QF}/\sigma_{\rm cap} \approx \int D_{\rm QF}dB$ (around 6% in the present calculation). This theoretical estimate may of course be refined by taking account of the different average values of R and B for the two processes (see Fig. 8).

C. Critical l for fission; the evaporation-residue cross section

Of course an E-dependence and/or an l-dependence can equally well be introduced into Eq. (19) and we consider here a second simple application of our results for the same system (compound nucleus ^{202}Pb). The survival probability $P_{\rm sur}(l, E^*)$ appearing in Eq. (28) can be calculated using a statistical-model code such as the HIVAP code of Reisdorf [10]. We use here a simple version of this program in which the level densities at the ground state and at the fission saddle point are fixed by the Toke and Swiatecki model of Ref. [28] and the l-dependent fission barrier is given by the liquid-drop model of Cohen, Plasil and Swiatecki [29], modified by an overall factor k in order to fit the experimental behavior of the critical angular momentum for fission. A satisfactory description of the data presented here is obtained with a typical value of $k = 0.7$.

The symbols in Fig. 10 show the HIVAP values of $P_{\rm sur}(l, E^*)$ as a function of l for ^{202}Pb at three different excitation energies: $E^*=51.25$, 53.75 and 56.25 MeV, corresponding to incident center-of-mass energies of 142,
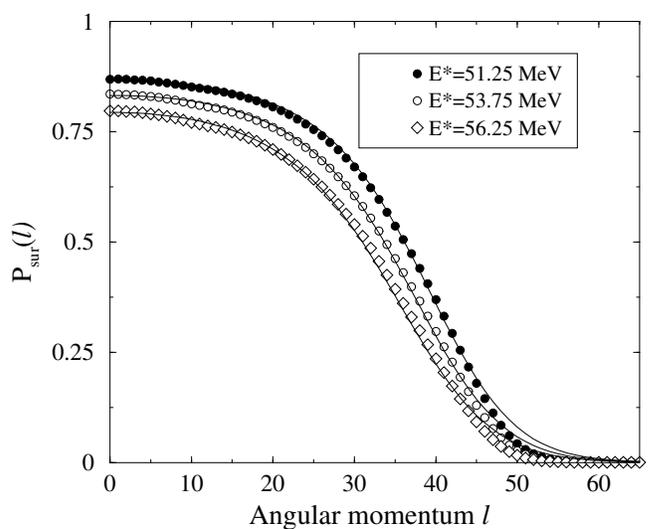

FIG. 10: $P_{\rm sur}(l, E^*)$ as a function of l for the ^{202}Pb compound nucleus at three different excitation energies $E^*(^{202}$Pb$)=$ 51.25, 53.75 and 56.25 MeV (corresponding to $E=142$, 144.5 and 147 MeV in the ^{48}Ca$+$ ^{154}Sm reaction). The symbols come from the HIVAP calculation described in the text. The solid curves are from the parametrization (30) with $[\gamma_{\rm sur}, L_{\rm sur}, \Delta_{\rm L}] = [0.91, 37.4, 21.7]$; $[0.89, 35.4, 21.7]$; $[0.87, 33.2, 21.7]$ in order of increasing energy. The upper and lower curves are used in the integral expression for $\sigma_{\rm ER}$, below 142 MeV and above 147 MeV respectively, with a linear interpolation between these energies.

145.5 and 147 MeV in the ^{48}Ca $+$ ^{154}Sm system. We see that this function changes with the excitation energy, though its overall shape remain the same. The solid curves show that the HIVAP results can be rather well fitted by the parametrization:

$$P_{\rm sur}(l) = \gamma_{\rm sur} \frac{1}{1 + \exp(\frac{l^2 - L_{\rm sur}^2}{\Delta_{\rm L}^2})}, \qquad (30)$$

with $[\gamma_{\rm sur}, L_{\rm sur}, \Delta_{\rm L}] = [0.91, 37.4, 21.7]$; $[0.89, 35.4, 21.7]$; $[0.87, 33.2, 21.7]$ in order of increasing energy. We have, therefore, fitted the ^{48}Ca$+$ ^{154}Sm evaporation residue by using this form of curve in Eq. (19).

In order to do so, we must transform to the variable E' whereupon we find

$$P_{\rm sur}(E') = \gamma_{\rm sur} \frac{1}{1 + \exp(\frac{E-E'-E_{\rm sur}}{\Delta_{\rm sur}})}, \qquad (31)$$

with

$$E_{\rm sur} = L_{\rm sur}^2/2mR^2 \qquad (32)$$

and

$$\Delta_{\rm sur} = \Delta_L^2/2mR^2. \qquad (33)$$

Note that the parameters $E_{\rm sur}$ and $\Delta_{\rm sur}$ now mix the properties of the CN with entrance-channel properties

through the factor mR^2. We take here a fixed value of $R = 11.96$ fm, which is just its value at the Bass barrier.

The theoretical curve in Fig. 9 shows that a good fit to the ER data can be obtained with a $P_{\mathrm{sur}}(E)$ having $[\gamma_{\mathrm{sur}}, E_{\mathrm{sur}}, \Delta_{\mathrm{sur}}] = [0.87, 4.4, 1.88]$ above $E=147$ MeV and $[0.91, 5.6, 1.88]$ below 142 MeV, with a linear variation of these parameters between these two energies. These values correspond to the solid curves in Fig. 10 at the corresponding excitation energies. We see that the energy variations from this simple HIVAP calculation fit the data rather well. However, our main point here was to show how the entrance-channel can be easily coupled to CN effects through a simple integral containing T_0^{tot}.

Of course it may be possible to create the same compound nucleus via several different reactions. In this case, $P_{\mathrm{sur}}(l, E^*)$ will be the same for each reaction but will have a different interplay with the different entrance-channels. These effects will be discussed in detail elsewhere [30], in particular for more fissile systems.

V. SPIN DISTRIBUTIONS

In the absence of quasi-fission, the spin distribution of the compound nucleus is simply given by the partial capture cross and in the spirit of this work we might write

$$\sigma_l \propto (2l+1)T_l \approx (2l+1)T_0^{\mathrm{tot}}(E'), \qquad (34)$$

with $E' = E - l(l+1)/2mR^2$. However, the main object of this paper has been to show how to reduce the size of coupled-channels calculations by performing them over a given energy range (up to where dT_0^{tot}/dE becomes 0) for a single angular momentum $l = 0$. This simpification is somewhat redundant if one wants a spin distribution at one or a few energies, when it is simpler to perform the calculations for all relevant l at the E in question, rather than to calculate T_0^{tot} at the same number of values of E'. Furthermore, each barrier will have a different R_α associated with it, whereas the above expression for E' incorrectly assumes a single value. (Note that we were able to account for the different R_α in Sect. III B only because we integrated over l.) Furthermore, high above the barriers, the l-dependence of the barrier position may also become important. Thus a direct coupled-channels calculation of T_l is recommended.

Although there are is no real advantage in using an expression such as (34) to evaluate the spin distribution quantitatively, it is still useful to think of this qualitatively in terms of arising from a barrier distribution. For example, we show in Fig. 11 the $(2l+1)T_l$ corresponding to the ^{100}Mo + ^{100}Mo calculation of Fig. 4. The solid lines are the CCFULL calculations at the energies indicated. It is clear that the steps in these functions arise from the different barriers in the distribution. High above a barrier we may write the corresponding critical angular momentum as $l_{\mathrm{crit}}^2 \approx 2\,m\,R^2(E - B)$, from which it is clear that the highest spins at any given E will always come from the lowest barrier, and that channel couplings
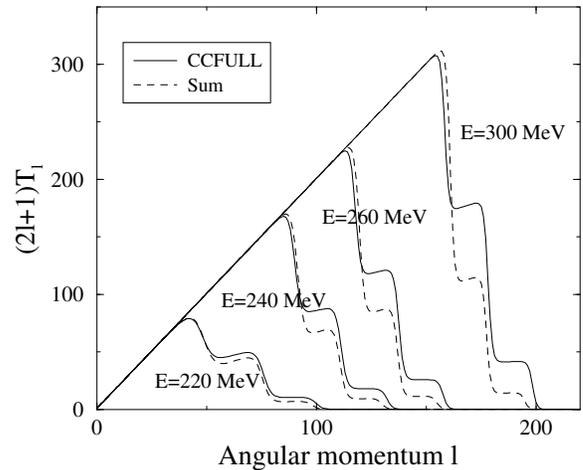

FIG. 11: Solid lines are exact CCFULL calculations of the spin distribution $(2l+1)T_l$ of the compound nucleus. Dashed lines are the sums of uncoupled optical-model calculations with barrier heights and weights defined for $l = 0$ (see Fig. 12 and Sect. VI). The discrepancies are relatively small for critical l values typical of high-spin state experiments, but show a significant variation of the barrier weights at high E (see Sect. VI).

will always increase the maximum attainable spin of the CN at a given incident energy.

Such considerations can be important when trying to form, for example, a hyper-deformed compound nucleus [31]. The hyper-deformed state will generally be formed only at rather high angular momenta, where there will be strong competition with fission. Coupling effects (giving rise to lowered barriers) allow us to attain the same high l at a lower excitation energy where this competition will be less severe.

VI. ENERGY DEPENDENCE OF THE WEIGHTS

Until now we have avoided the use of expressions like Eq. (4), since the (w_α, B_α) are not natural outputs of the CC equations. However, it is instructive here to try to use such an expression, since it will bring to light an important additional physical point. That is, in certain circumstances the weights associated with the barrier distribution may have a significant energy dependence. We shall illustrate this for the [1,1] calculation for ^{100}Mo + ^{100}Mo shown in Fig. 4. In Fig. 12 the solid line shows the exact T_0^{tot} for this calculation and the dashed line shows T_0^{tot} parametrized as a sum over barriers. The values of (w_α, B_α) used are: (0.038, 193.80); (0.295, 202.96) and (0.667, 212.30). For this case, the extraction of the weights is relatively simple since the peaks from each barrier do not strongly overlap. For more complicated couplings, for example higher phonon numbers, their extraction becomes more difficult; see solid curves of Fig. 1.

This can also be appreciated from the rotational calculation of Fig. 6, where the overlapping barriers also wash out the individual peaks. However, having obtained the relevant values one can use them to generate the full cross section, which is essentially indistinguishable from the solid curve in Fig. 4 a. We might, therefore, expect that the corresponding expressions:

$$(2l + 1)T_l \approx (2l + 1) \sum_\alpha w_\alpha \, T_l(E, B_\alpha) \qquad (35)$$

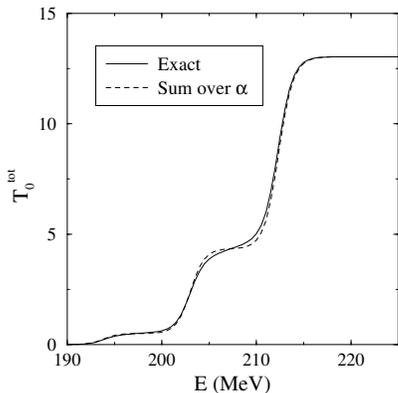will give a reasonable approximation to the spin distribution at an energy E.

FIG. 12: The exact T_0^{tot} (solid line) which corresponds to the system of Fig. 4, along with the sum of uncoupled calculations (dashed line) with the barrier weights and heights $(w_\alpha, B_\alpha) = (0.038, 193.80)$; $(0.295, 202.96)$ and $(0.667, 212.30)$.
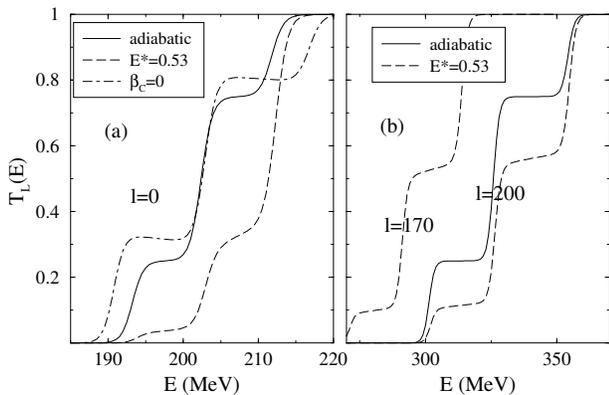

FIG. 13: (a) For a quadrupole phonon with $E^* = 0.53$ MeV, T_0^{tot} (dashed line) is very different from its adiabatic value (solid line) for $l = 0$, in particular the weight of the lowest barrier is greatly reduced. With no Coulomb coupling (dot-dashed line), however, the lowest barrier is actually enhanced relative to the adiabatic value. (b) For higher l, the barrier occurs at higher energy where the weights come closer to their adiabatic values. Calculations for $l = 170$ and $200\ \hbar$ show that the weights vary little over a limited range of angular momenta/energy.

Here, we could use the parabolic approximation for the

$T_l(E, B_\alpha)$, employing appropriate values of R_α and ω_α. Alternatively, we could calculate the $T_l(E, B_\alpha)$ directly with uncoupled potentials having the same diffuseness a as the original calculation, since this will reproduce more correctly the properties of each barrier (for example the variation with l). We choose to do the latter and the results of this procedure are shown by the dashed lines in Fig. 11. We see that while the positions of the steps are reproduced reasonably well, the heights of the steps are incorrect at higher energies. In other words the barrier weights appear to change as a function of the incident energy. Although this has a marked effect on the spin distribution, it has little effect on the total cross section which is summed over l.

It is clear from Fig. 12 that the weights and heights of the barrier distribution can be readily obtained from the steps in T_0^{tot} [33]. The B_α occur where T_0^{tot} rises most steeply, and the w_α are given by the differences between the steps in the function. (As noted above, this is less clear for smoother distributions.) How then can we define the weights at a higher energy, where T_0 has already become 1? The answer is to look at the same function but for a higher l value, for which the total potential barrier will occur around the energy in question.

This is demonstrated in Fig. 13 for the above system. Fig. 13 a shows T_0^{tot} calculated for the physical excitation energy of 0.53 MeV (dashed curve). One sees that the weights are very different from their adiabatic values ($E^* = 0$; solid curve). If one calculates the same function for an octupole phonon with the same E^* and β (not shown), the weights are close to their adiabatic values. The major difference between these two cases is the importance of the Coulomb coupling at large distances. In the quadrupole case, the range is long enough for the Coulomb coupling to strongly polarize the entrance channel before the barrier is reached [32]; clearly this coupling will favour the barrier for which the Coulomb field is lowest, that is, the *highest* of the barriers. This assertion can be confirmed by performing a calculation where the Coulomb coupling is switched off. This is shown by the dot-dash curve in Fig. 13 a. Now we see that the weight of the lowest barrier is actually enhanced (due to the nuclear couplings) relative to the adiabatic value.

In Fig. 13 b, we show T_l for $l = 200$, for which the barrier in the total potential (including the centrifugal term) occurs at around 325 MeV. The steps now give the barrier weights in this energy region. They are seen to be closer to their adiabatic values but still far from converged to these. We also show here the same quantity for $l = 170$ and see that the non-adiabatic weights do not vary significantly over the corresponding energy range. The reason for the slow convergence of the weights is that although the timescale associated with a 0.53 MeV excitation is relatively long, the long range of the quadrupole Coulomb field gives sufficient time for a strong polarization to take place even with an incident energy of more than 300 MeV.

A further interesting feature of Fig. 13 b is that the

energy difference between the highest and lowest barriers is significantly larger for $l = 200$ than for $l = 0$; around 53 MeV compared with 18 MeV. The reason for this is that the barriers for high l occur at a smaller radius than for $l = 0$, and in this region the nuclear coupling form factor is correspondingly larger. We note that this effect is specifically l-dependent rather than E-dependent.

The variation of the quadrupole Coulomb polarization is the origin of the discrepancies seen in the spin populations calculated with fixed weights in Fig. 11. We note that variations of the weights that we report here are larger than those discussed in Ref. [33]. However, there is no contradiction with these results, since the authors of that paper did not consider the long-ranged quadrupole Coulomb couplings and did not, in any case, study such a large energy range as here.

At energies near the $l = 0$ barrier, the quadrupole Coulomb field is the origin of the entrance-channel 'extra-push' energy described in Ref. [12], where the energy at which $T_0^{\text{tot}} = 0.5$ is increased by this polarization. For the present simplified [1,1] coupling scheme the shift is around $E_{\text{x}} = 9$ MeV (see Fig. 13 a) relative to the un-coupled barrier (a higher value is produced if multiple-phonon states are included in the coupling), significantly reducing the anomaly between the Bass barrier and the dynamical barrier observed in many symmetric heavy-ion reactions [12].

VII. CONCLUSIONS

We have presented new results relating to nuclear reactions which are governed by strong couplings in the entrance channel and, therefore, to the existence of a distribution of barriers. In some cases these effects can be easily incorporated into calculations of quasi-fission and evaporation-residue cross sections. This was achieved without the need to extract the heights and weights of the corresponding barrier distribution but simply by exploiting the the s-wave transmission coming from a standard coupled-channels calculation.

The only occasion on which we explicitly introduced barrier weights was to show that they may change with incident energy. But even in this case, the effect is important only for quadrupole-phonon states, only at energies high above the barrier and only in calculating the spin distribution of the compound nucleus rather than cross sections, which are summed over l. However, even at near-barrier energies, highly collective target and projectile quadrupole-phonon states can give rise to an important extra-push energy, that is, a significant shift of the average (dynamical) barrier to higher energies.

The reaction ^{48}Ca + ^{154}Sm was studied in some detail and, from a single T_0^{tot}, good results were obtained for the capture, quasi-fission and evaporation-residue cross sections, all of which been measured in this system. While the functions coupled with T_0^{tot} to give the ER cross section, have a good theoretical basis in the statistical-decay model, the function used to describe the quasi-fission was simply a generalization of the 'compactness' parametrization suggested in Ref. [17]. The data studied strongly suggest the correctness of this notion. It would, therefore, be good to have a theoretical model for this effect, especially since it appears to play a major role in systems leading to super-heavy element creation by hot fusion [34].

[1] S.S. Ntshangese et al., Phys. Lett. **B651**, 27 (2007).

[2] H. Ikezoe et al., in Proc. of FUSION06, Venezia, Italy 19–23 March 2006, Eds. L. Corradi et al., AIP Conference Proceedings **853**, 69 (AIP, New York, 2006)

[3] K. Hagino and N. Rowley, Phys. Rev. C **69**, 054610 (2004).

[4] N. Rowley, G.R. Satchler and P.H. Stelson, Phys. Lett. **B254**, 25 (1991).

[5] M. Dasgupta, D.J. Hinde, N. Rowley, and A.M. Stefanini, Ann. Rev. Nucl. Part. Sci. **48**, 401 (1998).

[6] H. Timmers et al., Nucl. Phys. **A633**, 421 (1998); A.M. Stefanini et al., Phys. Rev. C **76**, 014610 (2007).

[7] A.B. Balantekin and N. Takigawa, Rev. Mod. Phys. **70**, 77 (1998).

[8] L.F.Canto, P.R.S.Gomes, R.Donangelo, M.S.Hussein, Phys. Rep. **424**, 1 (2006).

[9] A.B. Quint et al., Z. Phys. **A346**, 119 (1993).

[10] W. Reisdorf, Z. Phys. **A300**, 227 (1981); W. Reisdorf and M. Schädel, Z. Phys. **A343**, 47 (1992).

[11] R. Bass, Phys. Rev. Lett. **39**,265 (1977).

[12] N. Rowley, N. Grar and K. Hagino, Phys. Lett. **B632**, 243 (2006).

[13] S. Bjornholm, W.J. Swiatecki, Nucl. Phys. **A391**, 471 (1982); J.P. Blocki, H. Feldmeier and W.J. Swiatecki, Nucl. Phys. **A459**, 145 (1986).

[14] C.Y. Wong, Phys. Rev. Lett. **31**, 766 (1973).

[15] K. Hagino, N. Rowley and M. Dasgupta, Phys. Rev. C **67**, 054603 (2003).

[16] N. Rowley, A. Kabir and R. Lindsay, J. Phys. **G15**, L269 (1989).

[17] D.J.Hinde et al., Phys. Rev. Lett. **74**, 1295 (1995).

[18] K. Hagino, N. Rowley and A.T. Kruppa, Comp. Phys. Comm. **123**, 143 (1999).

[19] C.L. Jiang, B.B. Back, H. Esbensen, R.V.F. Janssens,

K.E. Rehm, Phys. Rev. C **73**, 014613 (2006).

[20] H. Esbensen, Prog. Theor. Phys. (Kyoto), Suppl. **154**, 11 (2004).

[21] M. Dasgupta, in Proc. of FUSION06, Venezia, Italy 19–23 March 2006, Eds. L. Corradi et al., AIP Conference Proceedings **853**, 21 (AIP, New York, 2006).

[22] M.W. Cole and R.H. Good, Phys. Rev. **A18**, 1085 (1978).

[23] A.B. Balantekin, S.E. Koonin and J.W. Negele, Phys. Rev. C **28**, 1565 (1983).

[24] K. Hagino and Y. Watanabe, Phys. Rev. C, Rapid Communications, in press.

[25] A. M. Stefanini et al., Eur. Phys. J. **A23**, 473 (2005); M. Trotta et al., Eur. Phys. J. **A25**, 615 (2005).

[26] G.N. Knyazheva et al., Phys. Rev. C **75**, 064602 (2007).

[27] G.G. Adamian, N.V. Antonenko, W. Scheid and V.V. Volkov, Nucl. Phys. **A627**, 361 (1997) and references therein.

[28] J. Toke and W.J. Swiatecki, Nucl. Phys. **A372**, 50 (1981).

[29] S. Cohen, F. Plasil and W.J. Swiatecki, Ann. Phys. (NY) **82**, 557 (1974).

[30] N. Grar and N. Rowley, in progress

[31] B Herskind et al., Phys. Scr. **T125**, 108 (2006).

[32] A.S. Jensen and C.Y. Wong, Phys. Rev. C **1**, 1321 (1969).

[33] K. Hagino, N. Takigawa and A.B. Balantekin, Phys. Rev. C **56**, 2104 (1997).

[34] Yu.Oganessian, J.Phys.(London) G34 (2007) R165.